GEOPHYSICS, VOL. 72, NO. 2 (MARCH-APRIL 2007); P. WA105–WA116, 8 FIGS.
10.1190/1.2434798

Special Section — Marine Controlled-Source Electromagnetic Methods

Using CSEM techniques to map the shallow section of seafloor: From the coastline to the edges of the continental slope

Rob L. Evans[1]

ABSTRACT

Many important processes occur within the shallow section of the seafloor on the continental shelf and slope, yet conventional geophysical constraints on the physical properties within this critical boundary layer are limited. Some of the key constraints involve quantification of fluids within the seafloor, which can be provided by electrical methods. This paper reviews the application of a towed EM system to map the uppermost 20 m of seafloor in a variety of settings ranging from nearshore regions in water depths of approximately 10 m on the continental shelf out to water depths of 1300 m. The system is a mapping tool that provides areal maps of seafloor resistivity and has been used for a variety of purposes, including sedimentary characterization and facies mapping, evaluation of groundwater discharge, and mapping seafloor mounds in the Gulf of Mexico, thought to contain massive deposits of gas hydrate.

INTRODUCTION

The shallow section of the continental shelf is a key interface between the earth's crust and the ocean. This part of the seafloor provides a record of sedimentary history through the Holocene that can be interpreted in terms of changes in sediment supply and reworking. Important chemical fluxes pass through shallow sediments and into the ocean, including groundwater in coastal settings and fluxes of methane in deeper water.

Our knowledge of key sedimentary processes (i.e., transport, erosion, and deposition) and their spatial and temporal variability at the land-sea interface remains limited. One important piece in the solution of this puzzle is to build a shelf-wide picture of facies conditions and to link this to models of sediment supply and transport. From the oil industry's perspective some of the key features in the shallow section are analogs of features found deeper within the sedimentary section within oil fields (e.g., Gay et al., 2006). Chief among these are the nearly ubiquitous paleochannels, formed through fluvial incision during sealevel lowstands. Understanding the physical properties of shallow paleochannels can provide insights into their deeper counterparts and, in turn, help explain how these deeper features control oil migration. The shelf also represents a source of raw materials — particularly sand — that, if mapped, can be exploited, but it is also a delicate habitat that is just beginning to be understood.

The extent to which groundwater discharge occurs through subsurface routes across continental margins is a controversial subject. Estimates of the flux of water discharged range from a small to a moderate fraction of the freshwater discharged by rivers (see Church, 1996). Current means of detecting subbottom aquifer units and the discharge of freshwater are generally restricted to identifying appropriate chemical tracers that integrate over large areas (e.g., Moore and Shaw, 1998) and to pointing out active freshwater seepage (e.g., Swarzenski et al., 2001). Two key pieces of information can help improve our understanding of groundwater discharge in coastal settings. First, with the understanding that groundwater flow is controlled by regional geology comes the need to constrain not only the stratigraphic framework of a coastal plain aquifer but also its physical properties. Understanding how an aquifer extends offshore is important to proper management of supply. After all, interactions go two ways: Excessive pumping can lead to saltwater intrusion into a community water supply (e.g., Phillips, 1987). Second, physical properties measurements are needed that are sensitive to zones of freshwater. This is important not only to locate sites of discharge but also because offshore sources of potable water may become increasingly important as coastal aquifer systems become increasingly stressed.

In deeper water the flow of methane through the seafloor can be prevalent, sometimes resulting in the formation of shallow gas hydrates. The total volume of hydrocarbon held in hydrates has been

Manuscript received by the Editor April 24, 2006; revised manuscript received August 14, 2006; published online March 1, 2007.
[1]Woods Hole Oceanographic Institution, Department of Geology and Geophysics, Woods Hole, Massachusetts. E-mail: revans@whoi.edu.

suggested to be greater than the total hydrocarbon volume in other conventional hydrocarbon reservoirs (Kvenvolden, 1993), making hydrate a potential energy resource (Hovland, 2000). Methane is a powerful greenhouse gas. Although the amount of methane released through the seafloor that is able to enter the atmosphere is poorly constrained (Judd, 2004), the rapid breakdown of hydrate has been suggested to have impacted paleoclimate (Dickens et al., 1997). Finally, hydrates impact the shear strength of seafloor sediments by cementing grains together, whereas dissociation of hydrate has been suggested to cause slumps and slides. This is important because drilling in sediments containing hydrate may alter their physical properties to pose a hazard to drilling platforms (Hovland and Gudmestad, 2000).

This paper outlines how measurements of electrical resistivity are able to contribute to an understanding of these issues. Resistivity provides a first-order measure of seafloor porosity in sedimentary settings, allowing facies maps to be constructed or changes in lithology to be identified. In unconsolidated sediments, and to some extent in hard rock, porosity is a key parameter to understanding fluid transport. Resistivity is sensitive to the salinity of pore fluid, allowing identification of fresh groundwater. And finally, in areas of active gas seepage, there are often changes in pore-fluid salinity and temperature that resistivity measurements can identify, whereas accumulations of massive gas hydrate are thought to cause an increase in seafloor resistivity (e.g., Edwards, 1997).

We demonstrate specifically how resistivity can address these various targets by presenting data collected over more than a decade of research. The data presented were collected using two similar frequency-domain, towed magnetic-dipole systems [modified from the transient EM system of Cheesman (1989)]. Lawrie Law at the Geological Survey of Canada (GSC) operated the first system. The data presented in this paper were collected by the system operated by the GSC (working in the frequency domain) as well as by a second-generation system built at the Woods Hole Oceanographic Institution; the latter was based closely on that built by the GSC but with modifications to pressure housings and communications to improve deep-water operations.

The next section outlines the motivation for measuring the resistivity of the top 20–30 m of seafloor. The system used to make these measurements is described, and examples are given of where the system has been used. Finally, future developments and applications for the system are suggested.

RESISTIVITY OF THE SHALLOW SEAFLOOR

Within the uppermost seafloor the electrical resistivity structure is dominated by the presence of seawater in pores and interstices. This dependence arises because seawater has an electrical resistivity several orders of magnitude lower than that of the sedimentary matrix. If the seawater is distributed in a connected network, which is a good assumption except for the most indurated and diagenetically altered sequences, then this network will provide the path of least resistance for electric current flow.

Electrical resistivity has been used as a proxy for porosity in numerous small-scale studies of near-surface sediments recovered in coring operations (e.g., Andrews and Bennett, 1984; Wheatcroft et al., 1996; Jackson et al., 2002). Resistivity is most commonly related to porosity by Archie's law (Archie, 1942), which can be written as

$$\rho_m = A\rho_f\theta^{-m}, \quad (1)$$

where ρ_m is measured resistivity, ρ_f is pore-fluid resistivity, and θ is porosity. The term A is commonly used to describe the degree of saturation. We assume that all pore space is filled with seawater and set A to 1.0. Seawater resistivity at normal seafloor temperatures ranges from about 0.28 to 0.33 Ωm. Note that equation 1 does not contain any information on the resistivity of the sediment itself, which is several orders of magnitude higher. Instead, what controls the bulk resistivity (typically 1–10 Ωm) is the degree of interconnection of the pore fluid, described by the exponent m. Typical values of m are 1.5–1.8 for marine sands (Jackson et al., 1978; Jackson et al., 2002). Higher values of m in Archie's law reflect less well-connected, lower-permeability fluid distributions.

Although Archie's law was developed based on empirical observations, numerous numerical and theoretical studies show how a power-law relationship between resistivity and porosity naturally arises in fluid-bearing materials (e.g., Shankland and Waff, 1974; Madden, 1976; Wong et al., 1984; Roberts and Schwartz, 1985; Schwartz and Kimminau, 1987; Evans, 1994). Formal bounds on the conductivity of an isotropic two-phase material are given by the Hashin-Shtrikman bounds, which consider a suspension of isolated particles in a medium (Hashin and Shtrikman, 1962).

Grain-size variations and sediment type in the near surface are inferable through porosity changes, which, in turn, are quantifiable through measurements of electrical resistivity. In general, coarser-grained sands have lower porosities than fine-grained silts and clays. Uncompacted clays exhibit the highest porosities (typically in excess of 70%) (Hamilton and Bachman 1982; Wheatcroft et al., 1996) as the clay particles form an intricate and tortuous network.

Discriminating between sand types (porosities of about 30%–50%) on the basis of resistivity is difficult because the link between porosity and grain size in sands is not well defined. Although Hamilton and Bachman (1982) present an empirical relationship between mean grain size and porosity for sediments from the continental shelf (ranging in porosity from 30%–90%), Beard and Weyl (1973) point out that sorting plays a vital role in determining porosity. They show that for median grain sizes spanning those normal for sand grains, porosity is controlled almost entirely by the degree of sorting. Regardless of grain size, well-sorted sands have porosities of roughly 40%–45%, whereas poorly sorted sands span 25%–35% [see discussion in Evans (2001) based on data from Beard and Weyl (1973)]. How sorting influences resistivity is less well understood. Intuitively, at a given porosity, a poorly sorted sediment might be expected to be more resistive than one that is well sorted because the smaller grain sizes in the poorly mixed sample would tend to close conduction paths. Resolution of this issue will likely come through the careful collection of EM data along with detailed sampling and laboratory analysis.

Clays present a paradox, although identifying them on the basis of resistivity is more straightforward. The paradox is why such high-porosity, platy sediments have the most tortuous network (requiring a higher exponent in Archie's law) (e.g., Jackson et al., 1978; Andrews and Bennett, 1984; Martin et al., 1991; Jackson et al., 2002). For freshly deposited surficial samples with porosities in excess of about 70%, the Archie exponent m commonly approaches or exceeds 3.0. Although it is fairly easy to understand how a range of tortuosities might be possible for sediments with porosities less than about 50%–60% based on ideas of cementation, matrix support (Bennett et al., 1981), or differences in grain-size distributions, it is harder to understand this for high-porosity, small-grain-size sediments such as those associated with recent flood deposits.

Bennett et al. (1981) show through scanning electron microscopy how, at high porosities, extremely fine clay particles cluster around larger clay particles. These fine particles have a high affinity for the larger particles but allow chains of particles with a high void ratio to be formed. Such a structure looks, to some extent, like a series of closed pores (closed at least on several sides) and would explain the tortuosity associated with the electrical conductivity. However, such fine structure may not always be apparent without high-resolution imaging or be preserved without careful sampling of the sediments. Whether such structures are common, the effect they have on resistivity and the mechanism by which the larger grains are supported are not well understood. For example, if the bonding mechanism is electrostatic in origin, then this would have implications for how the sediment loses porosity with time through inherent weakening of bonds and also through wave action. Understanding the behavior of these high-porosity muds is important because they are known to damp wave energy in flat, mud-dominated coastlines such as those off Louisiana; by so doing, they ameliorate coastal erosion during high-energy storms (e.g., Sheremet and Stone, 2003).

Once compaction, consolidation, or diagenesis occurs, lowering porosity conduction relationships become more complicated. The elimination of conduction paths through precipitation and compaction has a dramatic impact on electrical resistivity. Studies of the change in conductivity and permeability resulting from the closing of pore spaces have been carried out for sedimentary rocks as well as for materials that act as analogs of compacting sediments (e.g., Bernabé et al., 1982; Zhang et al., 1994; Zhu et al., 1995). Models have also been developed to quantify the loss of connectivity upon compaction (e.g., Zhu et al., 1995). Both permeability and conductivity change with changing porosity according to a power law. There is typically a critical crossover porosity at which the behavior of the sample changes (often between 10% and 20%). At porosities greater than the crossover porosity the power law typically has a cubic relationship that reflects the tortuous nature of the pore space. Below the crossover point the conductivity starts to decrease much more rapidly with decreasing porosity. The crossover porosity represents the point at which connectivity starts to reduce within the rock network. In this case, the throats between adjacent pores become the critical transport property. As these throats become pinched or closed connectivity is lost and conductivity rapidly drops. The notion that conductivity has a threshold porosity necessary for conduction to occur has been studied in the laboratory (e.g., Bernabé et al., 1982). Although this is frequently seen for permeability, conductivity at low porosity is often controlled by secondary porosity (small cracks and fissures) that does not allow fluid flow but that is able to carry electrical current. This difference, as well as scaling differences between conductivity and permeability, makes it difficult to relate one to the other, even though both are transport properties (e.g., David, 1993). In the laboratory changes in porosity are realized by adding pressure, but closure of pore throats and networks can also occur by metamorphic reaction and deposition of minerals through fluid flow, although it is not clear that the two processes result in the same behavior at very low porosity (Roberts and Schwartz, 1985).

The conductivity of seawater, and hence the seafloor, is a strong function of temperature and salinity, which allows EM methods to identify regions of anomalous heat and/or fluid flux. From ambient seafloor temperatures to around 350°C the conductivity of seawater increases nearly linearly with temperature from 3 to around 30 S/m (Quist and Marshall, 1968; Nesbitt, 1993). Salinity also strongly influences seawater conductivity with a relationship that has also been well quantified through oceanographic use of the conductivity-temperature-depth (CTD) sensor (Perkin and Lewis, 1980). Highly saline brines are more conductive than fresh fluid. Because we know how the fluid resistivity changes with temperature and salinity we can use Archie's law to quantify the impact of different fluid flow regimes on the bulk resistivity of the seafloor.

Although there is ambiguity in differentiating changes in porosity from changes in temperature when using resistivity alone, the addition of resistivity as a physical property constraint in the kinds of areas discussed in this paper is advantageous in understanding the key fluid-flow processes taking place. At hydrate mounds, for example, it is possible to take heat-flow measurements to constrain temperature at a few points along a survey profile and allow the resistivity measurements to interpolate in between.

TOWED EM SYSTEM

Outline of system

The towed EM system discussed in this paper consists of three main components: the deck electronics, a transmitter, and the receiver string (Figure 1). The seafloor components of the system (transmitter and receivers) form a roughly 40-m-long array that is towed in contact with the seafloor at speeds of 1–2 knots (1 knot is roughly 0.5 m/s).

The EM transmitter, a horizontal magnetic dipole, generates harmonic magnetic fields over a range of frequencies, and the three receivers, tuned to measure these magnetic fields, are towed at fixed distances behind. At a given frequency the strength of the magnetic field decays away from the transmitter as a function of the conductivity of the seafloor (i.e., according to the skin depth), decaying more rapidly in more conductive media. Therefore, given that the frequencies are chosen appropriately, a measured signal will have primary sensitivity to changes in seafloor properties and will not be greatly affected by the overlying conductive seawater. The sensitivity of the magnetic dipole-dipole system, along with the physics of the propagation of the fields through the seafloor, is presented by Cheesman et al. (1987).

The deck electronics supply power to the system and allow real-time telemetry and control. Communications are accomplished through frequency-shift keying (FSK) in the very-low-frequency (VLF) band. Using two separate carriers, full-duplex communication is possible at 9600 baud both ways. The communication signals and power are combined onto a coaxial cable with a power separation filter (PSF). Communications are designed to work through as much as 10 km of properly matched, 0.680-inch coaxial cable. A software application allows commands to be sent to the system through the cable and also carries out logging and interpretation of the data, which happens in real time, with the data displayed on a shipboard computer.

The tow cable terminates at the transmitter, which contains reciprocal PSFs and communication boards to the ship. A pair of high-efficiency DC/DC converters provides +/−24 V, which is used to power the transmitter. The heart of the transmitter is a PC-104, responsible for controlling all underwater components of the system. This computer communicates with a CTD located just outside the transmitter pressure case. A bank of fiber-optic modems allows communications with the receiver string through a custom-made fiber-optic cable.

The rest of the transmitter is dedicated to analog electronics. Under the control of the PC-104, a signal is generated at the desired transmission frequency. This signal is amplified, and a relay board selects a combination of capacitors and coils for maximum output. These coils are located outside the pressure case and broadcast the signal through the seawater. The coils are protected by an outer plastic tube. The output power is up to 500 W. The seven transmitted frequencies are typically 200 Hz, 600 Hz, 2 kHz, 6 kHz, 20 kHz, 60 kHz, and 200 kHz, although the exact frequencies are determined by tuning the transmitter for optimal power output. The 2-kHz signal is measured by both the 40-m and 13-m receivers, and the 20-kHz signal is measured by both the 13-m and 4-m receivers. Once chosen these frequencies are fixed and typically do not alter between surveys.

The receiver string consists of three receivers, spaced 4, 13, and 40 m behind the transmitter. Each of these receivers is powered by an independent bank of 9-V batteries. The batteries are in an aluminum pressure case, whereas the rest of the receiver electronics are in plastic pressure cases rated to an ocean depth of around 3500 m. Both cases are housed in a tube of thick plastic to protect the system as it is dragged along the seafloor. Each receiver has a small coil inside the plastic pressure case which receives the signals from the transmitter. After amplification and filtering, the phase and amplitude of this signal is determined with a pair of homodyne receivers. Each receiver measures and logs amplitude and phase at three distinct frequencies, returning the measurements through the fiber-optic cable to the PC-104 controller and from there up the conducting cable to the ship. Each cycle of measurements (all three receivers) takes about 20 s to complete, corresponding to one measurement per receiver every 10–20 m along the seafloor, depending on tow speed.

In contrast to other seafloor EM methods, data collection with the towed system does not include time-series logging. Instead, amplitude and phases are determined in electronics, and the system is calibrated by its ability to measure the conductivity of seawater accurately, independently determined by the CTD. The system also operates at fixed source-receiver offsets at which signal levels are well above ambient noise levels and above the noise level of the magnetic coils in the receivers. One estimate of noise in the system comes from the reproducibility of the response between separate measurements; over regions of uniform seafloor conditions, this can be on the order of 1%–2% in terms of apparent porosity [e.g., see data from zone 1 in Evans et al. (1999)].

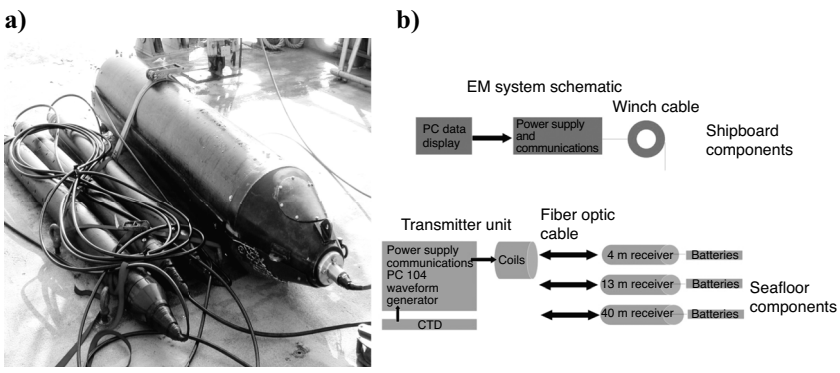

Figure 1. (a) Photograph of the EM system on deck. (b) Schematic of the system, showing its principal components. The system consists of three main components: the deck electronics, the transmitter, and the receiver string. The receiver string consists of three receivers, spaced 4, 13, and 40 m behind the transmitter coils. The seafloor components are towed in contact with the seafloor at speeds of 1–2 knots.

To date, navigation of the system has relied on estimating the layback of the system from the ship based on water depth and wire out. For most shallow-water applications this is reasonable. In deep water, layback calculations can be more error prone, although the navigation of data from the Gulf of Mexico shown in a later section appears to be accurate to about 50 m. In a recent survey a short baseline transponder was mounted to the system, improving the estimation of seafloor positioning.

Advantages of system

Two key choices in the design of the system bear some discussion. The first is that it is a horizontal magnetic dipole-dipole (HRHR) array, and the second is that it operates in the frequency domain. The horizontal electric dipole-dipole (HED) configuration has become the most widely used setup for marine CSEM, both for large-scale (e.g., Cox et al., 1986; Evans et al., 1991, 1994; MacGregor et al., 1998, 2001; Weitemeyer et al., 2006) and small-scale surveys (Cairns et al., 1996; Yuan and Edwards, 2000; Schwalenberg et al., 2005), although there are (to our knowledge) no HED systems that operate at the same spatial scale as our magnetic system. The primary advantage of a magnetic setup is that it permits the entire system to move continuously while making measurements. Moving electric-dipole receivers are prone to noise from streaming potentials caused by the motion of the electrodes in conductive seawater. Although the magnetic source is a little more complicated and bulky than an electric-dipole, in practice, the coil housing protects the pressure case that houses the power supply and communications electronics as well as the CTD.

The choice of frequency domain over time domain is also somewhat logistical in nature. In practice, it is fairly straightforward to transmit a sequence of frequencies that are well chosen to provide appropriate information on the seafloor at each receiver. The amplitudes and phases of these fields are measured by the electronics within the system so that the data displayed in real time on boardship are representative of the seafloor (the three amplitudes and phases measured by each receiver are converted to apparent resistivities and, from there, to apparent porosity using equation 1). As we show later, inversions of data from all three receivers are sufficient to produce a smooth resistivity-depth profile that agrees well with observations of structure either from cores or from logging-while-drilling data. Choosing frequency domain minimizes the amount of information that must be logged and stored.

Because the system maintains a fixed distance between source and receiver, it can be regarded as a mapping tool. To build a map of subseafloor structure only relatively sparse (compared to chirp seismic) coverage is needed (e.g., Evans et al., 2000). The resulting map (Figure 2) provides spatial coverage superior to conventional coring techniques (approximately one measurement every 10–20 m) and can measure porosities in regions where coring techniques fail to recover samples. More importantly, it provides a means of interpolating between discrete core locations. (Further discussion of Figure 2 is in the "Seafloor Characterization" section). Finally, the method provides estimates of physical properties where seismic reflection profiles are contaminated by

strong bottom multiples or the presence of biogenic gas (Cheesman et al., 1993). The system is, however, perfectly complementary to seismic methods and is best used in concert with high-resolution seismic reflection techniques that define the stratal geometry while the EM data define the physical properties (e.g., Mosher and Law, 1996; Evans and Lizarralde, 2003; and examples below).

Both frequency- and time-domain EM generally provide greater sensitivity to seafloor structure than standard dc resistivity methods adapted for the oceanic environment. Over resistive seafloor, at low-frequency or DC conditions, most of the applied current flows through the seawater, so, even substantial changes in the seafloor resistivity have only a small effect on the fields measured. The towed system is able to identify changes in surface apparent porosity (averaged over the top 1–2 m of seafloor) of about 1%–2%, and these apparent values compare well with those measured in cores and sediment samples (e.g., Evans et al., 1999; Evans, 2001; Ellis et al., 2005).

Finally, EM propagation in the oceanic environment is a diffusive process, which precludes the technique from obtaining the same kind of detailed spatial images provided by seismic reflection profiles or from core logging. However, the method does provide estimates of the bulk physical properties of the seafloor, both laterally and vertically, over depth ranges that seismic methods are not well equipped to address. These bulk properties can be incorporated into a joint geophysical and geological analysis and, as such, are more akin to refraction seismology. Because of the data sampling rates, the system is able to constrain structural variations with horizontal wavelengths on the order of a few tens of meters.

DATA PRESENTATION AND INVERSION

A single set of amplitude and phase measurements (three frequencies at one receiver) of the transmitted magnetic field can be modeled in terms of an apparent resistivity, which is the resistivity of the uniform half-space that would produce the observed response. As the system is towed along the seafloor it produces a series of apparent resistivities at intervals along the tow line. Each apparent resistivity is in some sense an average of the resistivity over a local volume surrounding the source and receiver. The apparent resistivities can be converted to apparent porosity using equation 1. By examining the apparent resistivities or porosities along track and between the three source-receiver pairs, it is possible to build a porosity pseudosection (Figure 3; see the Eel River section).

For the most part, interpretations can be based largely on the apparent porosities that appear in real time on shipboard, either in profile form or in the form of apparent porosity maps (Figure 2; see "Seafloor Characterization" section). However, in some cases it is desirable to invert the data to estimate true porosity with depth. We have used two inversion schemes: (1) a standard Occam inversion (e.g., Constable et al., 1987; Parker, 1994) that solves for a smooth conductivity model and (2) an L1-norm inversion (Bailey and Cheesman, 1992) that uses linear programming to minimize the sum of the absolute values of the model properties. The L1-norm solution essentially consists of the model with the least number of layers that satisfy the data, although the model is, as for the Occam solution, overparameterized, so the choice of the number of model layers is not required a priori. The choice of which approach to take depends on the setting. In most sedimentary environments the resistivity generally changes smoothly with depth; so, for the most part, the Occam solution is preferred. However, there are instances (see "North Carolina" section) where the sharp contacts and changes in lithology with depth would make an L1-norm approach more suitable. Because of the limited length scale of the system we have so far only conducted inversions for a layered structure. Although there are clearly areas of seafloor with 2D or 3D structure, in practice, it has proven possible to extract measurements at locations where a 1D approximation is valid.

An ubiquitous issue with inverting geophysical data is the estimation of data uncertainties and the level of misfit to which the data should be fit. Estimates of noise on the EM system come from calibration runs within the water column during which many repeat measurements are made. However, these estimates do not represent other sources of noise in the data such as might be caused by seafloor roughness, misaligning the source and receiver, small-scale geologic heterogeneity, or two- and three-dimensionality in the data. The example shown in Figure 4 is an Occam inversion of data from the Gulf of Mexico (see Gulf of Mexico section). The preferred inversion model compares favorably to adjacent logging-while-drilling measurements (Collett et al., 2005). To obtain this model we have inverted data at decreasing levels of misfit while tracking the model roughness. This approach is not new; it is discussed in Parker (1994) and has been used in inversions of larger-scale CSEM and MT data (e.g., MacGregor et al., 1998; Baba et al., 2006). In this example, however, it is satisfying to see that the choice of misfit based on the roughness-misfit versus trade-off curve (Figure 4) is also the model that best matches the drilling data. Further examples of inversion of

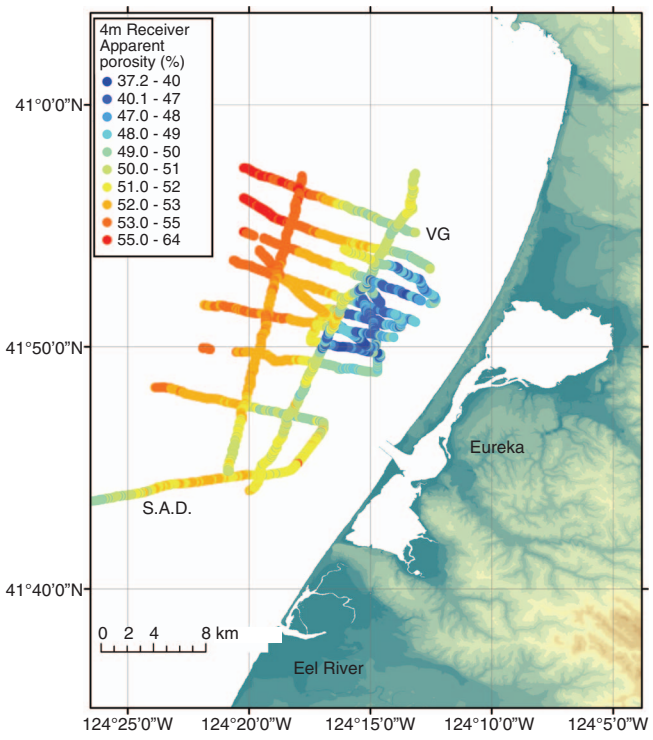

Figure 2. A porosity map based on data from the 4-m receiver collected across the Eel River Shelf (Evans et al., 1999). Symbols reflect apparent porosity values as shown in the legend. The background map shows elevation of northern California with the town of Eureka marked for reference. The Eel River is the primary source of modern sediment to the system. The line through the subaqueous delta (S.A.D.) is used to construct the pseudosection in Figure 3. Data from the northern profile (VG) are used to construct the semivariogram in Figure 5.

data from the EM system compared to porosities from cores are given in Evans (2001).

SEAFLOOR CHARACTERIZATION

The use of the towed EM system for seafloor characterization relies on the ability to identify and map regions of seafloor of distinct sediment type. Resolution within the uppermost few tens of centimeters of seafloor has been investigated in detail by Evans (2001). Most attempts at characterizing seafloor type use acoustic backscatter methods. The problem with this approach is that backscatter is influenced not only by grain size and distribution but also depends heavily on seafloor roughness and near-surface heterogeneities (e.g., Jackson and Briggs, 1992). Furthermore, the impact of muds and sands on backscatter amplitude can be very different. For example, on the Eel River shelf off northern California the highest backscatter (Goff et al., 1999) is seen in the area of highest porosity (Evans et al., 1999).

In contrast, and counterintuitively, the sandy, low-porosity subaqueous delta of the Eel River shows very low backscatter. Evans (2001) shows how the addition of porosity measurements from the EM system allows the discrimination of muddy regions from sandy regions. For example, in Figure 2, southern and nearshore areas of lower porosity represent sandy environments, whereas the higher-porosity region in the northwest is the locus of recent muddy flood deposits. A more recent data set collected off Martha's Vineyard, Massachusetts, a sandy setting with abundant sand waves and ripple fields with length scales of tens of centimeters (Goff et al., 2005), shows no obvious correlation between surficial porosity (as measured by the EM system) and acoustic backscatter, although Goff et al. (2005) claim to see a link between grain size and backscatter, albeit complicated by apparently different behavior of fine- and coarse-grained sands. This complexity may reflect the influence of ripple fields on acoustic backscatter signal, with larger-scale (wavelength and amplitude) ripple fields found in coarser-grained sandy environments.

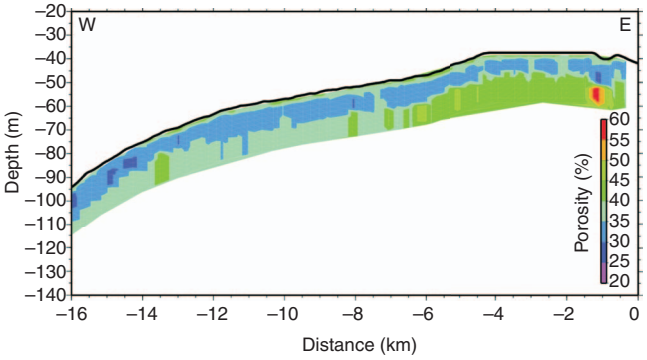

Figure 3. A porosity pseudosection of data collected on the Eel River Shelf within the subaqueous delta [see Figure 2 and Evans et al. (1999) for details of coverage]. The top surface is the depth below the sea surface; the depths below that are pseudodepths. The data are contoured assuming that the depth of penetration is one-half the source-receiver offset, with interpolation to produce a smooth porosity-depth profile. This profile shows a buried low-porosity layer at a depth of about 5 m and with a thickness of about 10 m underlain by a higher-porosity substrate. The unit is roughly coincident with the area of low acoustic backscatter (Goff et al., 1999) associated with the subaqueous delta. In terms of the raw data the apparent porosities on the 40-m receiver are elevated above those of the 13-m receiver.

Analysis of sidescan data and grab samples from the New Jersey shelf also show correlations between backscatter and grain size, with highest backscatter coming from coarsest-grain sediments (Goff et al., 2004). EM data from the same region generally concur with this. For example, across sediment ridges whose peaks are high-backscatter environments thought to contain abundant shell hash, the porosities decrease (Evans, 2001). However, there is no systematic trend in porosity across the ridges that might be related to models of grain-size sorting across these features. This brings us back to the issue raised above about the relationship between grain size and porosity, one that will likely only be solved through acquisition of further data sets and colocated samples.

The high spatial density of measurements obtained by the EM system allows detailed statistics of seafloor variability to be calculated. One approach to estimating sediment variability and bedform wavelength is to calculate a semivariogram that shows the absolute change in physical properties compared to offset distance. Over a uniform seafloor there will be no change in properties with increasing offset. In contrast, if measurements are made in a region with a distinct change in properties, then the variogram will show a trend over a length scale related to the scale of the bedform before reaching a plateau. Typically, these kinds of plots are made from surface samples or cores (e.g., Goff et al., 2002, 2004). But such data are usually

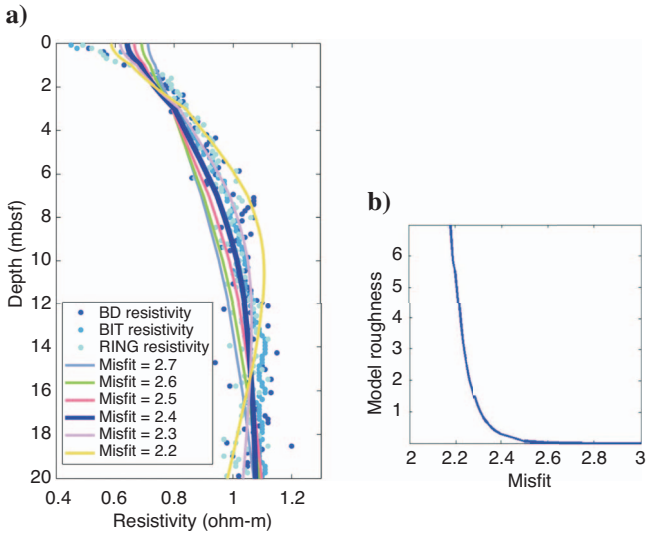

Figure 4. (a) Inversion of EM data from the AT-13 site, Atwater Valley, northern Gulf of Mexico (Ellis et al., 2005), compared with JIP drilling data. The smooth lines are models resulting from a regularized inversion of data from the EM system (13-m and 40-m receivers). We have systematically run inversions at decreasing levels of misfit and examined the misfit-roughness curve (b). A value of 2.4 is considered an optimal choice on the basis of fit and roughness (dark blue model), although models close to this misfit value are also acceptable. The preferred model provides a satisfactory agreement with logging-while-drilling data shown in (a) by the blue dots, although again other models close to this misfit value also agree well with the logging data in places. The scatter in the logging data reflects the different tools used (referred to as BD, BIT, and RING), which have different scales of sensitivity but are all on the order of ~1 m. The logging tools also sense small-scale features that the EM system cannot resolve. Note that the loss of resolution in the uppermost 1 m of the model is related to the lack of data on the 4-m receiver, which failed during the deployment.

limited in terms of sample density, forcing averaging and binning of data. For example, where Goff et al. (2002) analyze 100 samples off New Jersey, the EM system has more than 20,000 measurements in the same area. This allows us to examine the statistical distribution of data within the variogram. It also allows us to maintain constant range bin sizes across the offsets spanned by the data but still maintain reasonable representative populations within each interval. A variogram from the Eel River (Figure 5) shows the trend in porosity as data are collected in two distinct environments: one, the high-porosity but spatially uniform flood deposit; the other, a nearshore sand zone. The distribution of porosity changes within a given range bin are non-Gaussian and can be approximated by a gamma distribution with a mode smaller than the distribution mean and with a long tail and frequent outliers.

Lithology

The clearest example of how the system responds to changes in lithology comes from Long Bay, North Carolina (Evans and Lizarralde, 2003). Here, a variable sediment cover overlies a hard limestone unit thought to be the Eocene Castle Hayne, one of the main regional aquifer systems providing drinking water to the Wilmington area. Coincident EM and chirp seismic profiles were collected over an area of locally punctuated, high-flux submarine groundwater discharge 20 km offshore North Carolina. The seismic profiles allow the identification of stratigraphic units, whereas the EM tool responds to changes in physical properties. The location is strongly affected by karstification caused by the discharge of chemically distinct groundwater to the seafloor (Moore et al., 2002). The profile shown in Figure 6 is an example of the data collected in Long Bay. Toward the southern end of the line (3200–3650 m) is a striking seismic reflector that also corresponds to a dramatic drop in porosity on the 40-m receiver. This reflector is almost certainly a dense, relatively impermeable limestone block with a gently dipping top surface and steep sides.

Paleochannels

Towed EM surveys have been carried out in three regions containing paleochannel sequences: New Jersey, where channels were formed by fluvial incision during a sealevel lowstand in the midshelf (Evans et al., 2000); North Carolina, where a series of fluvial channels incise down to the top of a limestone aquifer; and offshore Martha's Vineyard, Massachusetts, where a series of shallow channels are thought to represent the offshore extension of onshore valleys formed by glacial sapping processes (Uchupi and Oldale, 1994). The channels generally show higher apparent porosities than the surrounding seafloor into which they are carved, reflecting either the higher porosity of lag deposits that infill them with time or the loss of small grain size material through advection. An example of channel sequences from North Carolina is shown in Figure 7 (see North Carolina section).

Paleochannels are important features in continental-shelf petroleum reservoirs because the typically coarser-grained fill acts as a high-permeability conduit for oil and gas migration. As an example, Gay et al. (2006) use 3D seismic data to map a volume of shelf within the Congo Basin. Here, a sequence of vertically stacked, turbiditic paleochannels is overlain by a series of apparently related seafloor pockmarks and seismic chimneys, suggesting that these channels have focused fluid flow. Although the features within an oil field are typically too deep to be imaged using the towed EM system, we can study shallower forms in some detail and use the information to provide insight into the oilfield analogs.

In 1998, we completed an EM survey (Evans et al., 2000) across two portions of the sediment-starved New Jersey continental margin, shown to contain buried paleochannels (Davies et al., 1992; Davies and Austin, 1997). The bulk-porosity estimates provided by the EM system constrain the nature of the channel infill and the contrast in physical properties across the channel boundaries. A distinct EM response was seen in one set of buried channels that had been imaged seismically (Davies and Austin, 1997). These channels carve an unconformity thought to represent a subaerially eroded surface exposed during the late Wisconsinan glaciation. This unconformity has been buried by an outer-shelf wedge of sediment, although the channels seen are on the periphery of this wedge where it attains a thickness of only 2–3 m (Milliman et al., 1990). The EM responses of these channels are consistent with structures about 7–10 m deep, with a high-porosity lag deposit a few meters thick lining their bases.

Another sequence of paleochannels has been imaged off the south shore of Martha's Vineyard, Massachusetts. Unlike the channels off New Jersey, these features are not thought to represent fluvial channels but instead are the offshore extension of glacial sapping valleys, widespread throughout the region (Uchupi and Oldale, 1994). Sapping is defined as "the process that causes the undermining and collapse of a slope by weakening or removal of basal support by weathering and erosion by fluid flow at the site of seepage" (Laity and Malin, 1985; Baker et al., 1990; Uchupi and Oldale, 1994). A large number of linear valleys seen in Upper Cape Cod, Massachusetts, and on the south shore of Martha's Vineyard have been interpreted as sapping channels associated with the Laurentide ice sheet (Uchu-

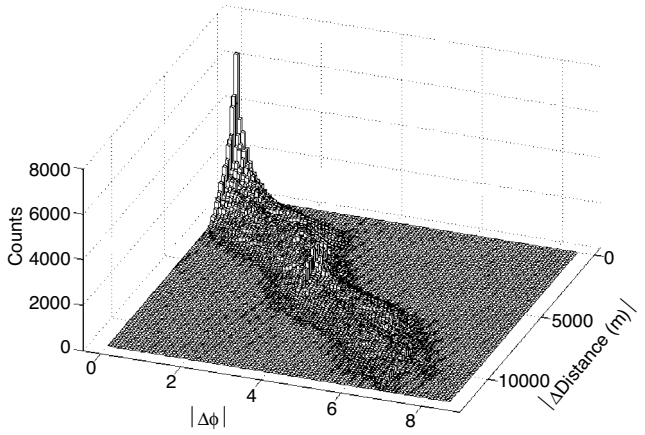

Figure 5. A variogram for data collected in the northern portion of the Eel River shelf (Figure 2; Evans et al., 1999). The variogram is formed by calculating the absolute difference in apparent porosity $|\Delta\phi|$ between all combinations of pairs of measurements on the 4-m receiver and plotting this value as a function of absolute Euclidean distance between the measurement locations. Over a uniform seafloor there would be no trend in $|\Delta\phi|$ with increasing distance. In this case, a trend is seen, although the variogram does not plateau, suggesting that the data do not sample the complete range of structure. The plot shows the variogram as a 3D histogram; this is useful to examine the distributions of the data, which are generally seen to be non-Gaussian (true for data on the Eel River, New Jersey, and off Martha's Vineyard). The data are partitioned into 100×100 bins of equal size determined by the maximum and minimum offset and porosity values. These are approximately 120 m in offset and 0.1% in porosity.

pi and Oldale, 1994). The transport of meltwater from a proglacial lake through the permeable outwash deposits to its release at a scarp or free slope resulted in steep-sided, flat-floored, linear valleys. Erosion of the valleys moved headward toward the proglacial lake until the lakes drained and the water table fell below the valley floors. The valleys flooded as sea level rose through the Holocene. The southern shoreline of the island now features a barrier beach system, which fronts the coastal ponds that mark the onshore portions of the valleys. The area has been widely studied as part of the Office of Naval Research's mine burial prediction program. Seismic profiling, high-resolution acoustic mapping, and coring have been carried out in addition to the EM survey (Goff et al., 2005). EM lines that run parallel to the shoreline reveal the signatures of the buried valleys through raised porosities on the 4- and 13-m receivers. Similar channel responses are seen in seismic reflection profiling, although penetration in this shallow-water, sandy environment was not good. The channels are generally quite shallow, extending only a few meters into the subbottom, and the porosity contrast between the infill and the surrounding outwash-plain sediment is not large (5%–10%); yet, as the system passed adjacent to one of the offshore ponds, a clear signal was seen.

Buried resistive layer: Eel River subaqueous delta, northern California

Seafloor resistivity profiles were measured along 120 km of tow line on the Eel River shelf off Humboldt Bay, California, from water depths of 30–100 m (Evans et al., 1999). Within the confines of the Eel River subaqueous delta is a buried resistive layer, about 5–10 m thick, underlain by a more conductive substrata (Figure 3). The origin of this layer is uncertain, although the most likely explanation is that it represents the paleodepocenter of muds released from the Eel River under different sea-level conditions than today. These muds would have been deposited on top of sands laid down during sea-level lowstand and would represent the earliest formation of the subaqueous delta. The muds might act as an impermeable boundary preventing the dewatering of the underlying sands, explaining the increase in conductivity at depth.

COASTAL GROUNDWATER DISCHARGE

The identification of freshwater-bearing aquifers or permeable units into which meteoric water can penetrate and mix with seawater is hard using traditional geophysical methods. EM methods promise to be able to constrain hydrologic conditions in the upper-most seafloor by identifying the lithologic structure that controls the permeability, zones of high porosity, and zones of freshwater as anomalously resistive units (Hoefel and Evans, 2001).

Eel River shelf

On the inner Eel River shelf off northern California in water depths less than 60 m, the electrical structure exhibits a high spatial variability, with apparent porosities less than 20% — in some places as low as 10% on the 40-m receiver (Figures 2, 3, and 5). The low porosities extend upwards to within a few meters of the seafloor. There are several explanations for the high resistivities. The first is that high resistivity is caused by diagenesis associated with the formation of a large anticline system just to the south of the low-apparent-porosity region, the nose of which reaches to within a few meters of the seafloor. Another possibility is that the anticline system is channeling freshwater offshore and discharging it through the seafloor. For example, a reduction in salinity to 9.4 ppt (water conductivity of 1.0 S/m) would mean that sediment with a true porosity of 40% would be predicted as having a porosity of only 17%. Fresher porewaters would cause us to underpredict the porosity (based on examination of apparent porosities) by a larger margin. Although these salinities may seem low, they are consistent with samples from several places along the Atlantic margin where salinity-depth profiles through areas of freshwater discharge have been measured (see Hoefel and Evans, 2001).

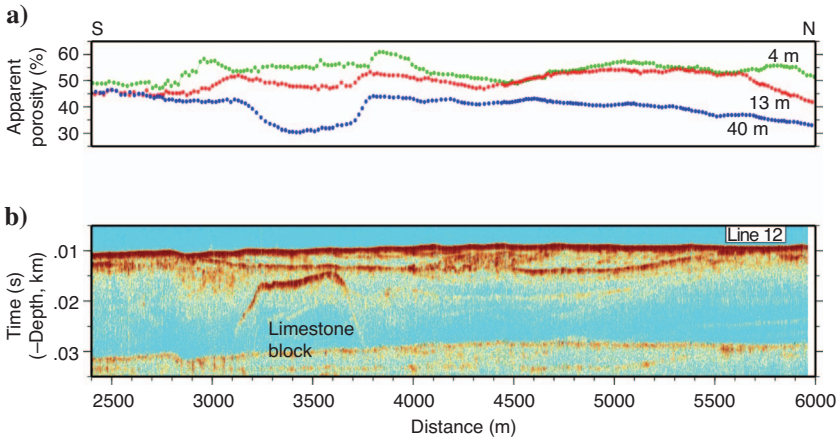

Figure 6. (a) EM data and (b) a coincident chirp seismic profile from Long Bay, offshore North Carolina (Evans and Lizarralde, 2003). The EM data are plotted as apparent porosity, one for each receiver (green, 4 m; red, 13 m; blue, 40 m), which is as they would appear in real time on shipboard during a survey. These data clearly show the impact of buried lithological contrasts on the EM, with the raised limestone bench reflected in the reduction in apparent porosities on the 40-m receiver, which is the deepest probing (excerpt from Evans and Lizarralde, 2003).

North Carolina

Paleochannels filled with high-porosity material can act as high-permeability conduits between land and ocean to facilitate enhanced exchange of groundwater. Hydrologic modeling of a coastal-plain setting, which includes a confined aquifer breached by a paleochannel, highlights the role of these features in modulating groundwater exchange. The modeling shows how discharge is concentrated along the margins of the channel, while recharge of seawater occurs along the channel axis to result in higher salinity in the middle of the channel relative to the flanks (Mulligan, 2007). Modeling also predicts that the freshwater/saltwater transition zone is closer to land below paleochannels than in locations with a continuous confining unit. Such channels are likely to be significant modes of saltwater intrusion into confined aquifers when excess freshwater extraction occurs on land. A combination of seismic and EM data were collected off Carolina

and constrain the geometry of the principal hydrologic units as well as their physical properties (Figure 7). The primary unit is the low-porosity Castle Hayne limestone, which appears as a resistor, thus lowering the apparent porosity of the 40-m receiver. Along-shore profiles show considerable variability of porosity mainly associated with the channel sequences in the area. However, the hydrologic modeling nicely captures the response on the 4- and 13-m receivers, which show freshening along the channel walls with more saline fluids in the channel flanks at a distance of about 1 km from shore (Figure 7a). Farther from shore (Figure 7b), the channel sequences have a more characteristic response, with raised apparent porosities within their confines and even the suggestion of higher-porosity lag deposits at the base of the channel.

GAS SEEPS AND GAS HYDRATE ACCUMULATIONS

Gas hydrate distributions within sediments on the continental margins have important ramifications for the global carbon budget, for climate, as future energy resources, and for slope stability (e.g., Kvenvolden, 1993). Studies of methane gas hydrate reservoirs along a number of continental margins have mapped the important zones within these reservoirs (sulfate-reduction, hydrate-stability, and free-gas zones) and have begun to develop a flux-based framework for understanding the variations between these zones observed in different settings (Xu and Ruppel, 1999). High-resolution geophysical techniques that image this important shallow region of gas hydrate reservoirs hold great potential for providing measures of the regional flux conditions, but large uncertainties remain about how hydrates are distributed within seafloor sediments, the importance of localized concentrations of hydrate, and the role that focused fluid flow plays in controlling these localized concentrations.

Occurrences of shallow and outcropping hydrate as well as accompanying gas seeps are common in the Gulf of Mexico, are found over a variety of water depths, and constitute a dynamic environment that changes on a timescale of months to years (e.g., Brooks et al., 1984; Kennicutt et al., 1988; Sassen et al., 1998). A full understanding of the processes governing hydrate distribution and evolution with respect to fluid expulsion requires a multifaceted, interdisciplinary approach. In particular, methods are needed that can provide maps of subbottom physical properties that can discriminate the presence of hydrate and link these distributions to faults because shallow hydrate accumulations require high methane fluxes that can only be supplied reasonably through cracks and faults. Sampling through submersibles or coring are able to provide point measurements of hydrate, but covering large areas with such methods is expensive. Although EM experiments have been carried out to measure hydrate abundances through the hydrate stability zone, which typically extends to depths of 100 m to several hundred meters below the seafloor (Yuan and Edwards, 2000; Schwalenberg et al., 2005; Weitemeyer et al., 2006), these methods do not have sufficient spatial resolution to map shallow hydrate occurrences within the sulfate-reduction zone in the top few tens of meters of seafloor.

The solid ice-like nature of massive hydrate suggests that these features should be electrically resistive (Edwards, 1997). However, locations of hydrate accumulation at the seafloor are, by definition, sites of high methane flux (Xu and Ruppel, 1999); therefore, they are also sites of advective fluid flow that can raise temperatures. In addition, in places such as the Gulf of Mexico, these fluids may have raised salinities (e.g., Ruppel et al., 2005), and in other locations, such as Hydrate Ridge off the coast of Oregon, the formation of shallow hydrate results in the exclusion of salt to yield interstitial brines (Milkov et al., 2004). These additional factors complicate the resistivity around gas seeps and hydrate formations. Recent work in the Gulf of Mexico suggests that fluid advection through the seafloor is more prevalent than would be suggested by merely looking for mounded structures as evidence of expulsion (Wilson and Ruppel, 2005).

EM data from hydrate mounds in the Gulf of Mexico

In 2004, EM data were collected in Atwater Valley in the Gulf of Mexico at about 1300 m water depth. The site features two mounds that were drilled as part of an industry-academia (JIP) partnership in 2005 (Collett et al., 2005). The two mounds (D and F) both have about 10 m of relief and lateral extents of 100–200 m. Amplitudes of acoustic reflections from the seafloor on the mound are brighter than those from adjacent seafloor, suggesting possible hard-bottom conditions associated with hydrate and/or authigenic carbonates. Deeper-looking seismic reflection data show disturbances in the underlying seismic stratigraphy which suggests advection of gas and/or fluids from depths toward the mound. It has been suggested that hydrate might be stable within the mound, and this prediction is apparently supported by proprietary cores containing hydrate that have been recovered from the mound.

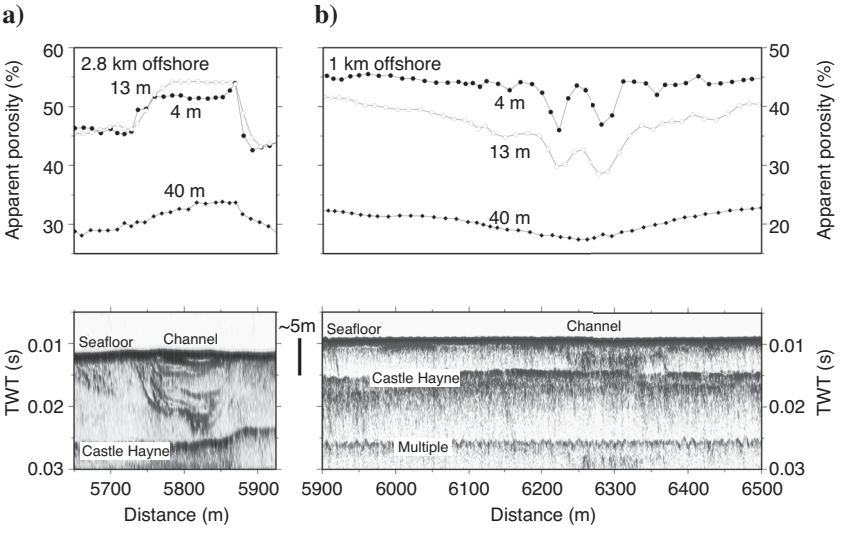

Figure 7. Examples of paleochannels off North Carolina. The channel 2.8 km from shore (a) shows a typical channel response with higher apparent porosities within the confines of the channel, most likely caused by coarser-grained channel lag deposits. The channel 1 km from shore (b) shows a more complex response. Hydrologic modeling suggests that the drop in apparent porosities, particularly those on the 4-m and 13-m receivers, is caused by freshwater leaking from the Castle Hayne aquifer through the channel flanks and into the ocean (Mulligan, 2007).

EM profiles were collected continuously for about 17 hours on nine lines. EM data showed raised apparent porosities across both mounds and also at discrete locations on the surrounding seafloor (Figure 8). The explanation for the raised porosities is a combination of raised pore-fluid temperatures and salinities beneath the mounds (Ellis et al., 2005). This interpretation is supported by heat-flow data and coring as well as by the drilling results. Inversions of models obtained on and off the mound compare well with resistivity-log data measured during a drilling program (Collett et al., 2005; Figure 4). In addition to anomalies seen across the two mounds, there are other locations, possibly coincident with fault structures seen on sidescan, where the apparent porosities increase. These may be other loci of fluid expulsion. Although the data set collected is not able to place constraints on the spatial scale of this flow, they do suggest that, with proper surveying, the EM system should be able to help constrain patterns of shallow flow. In Atwater Valley, the impact of hydrate, if present at all, on the resistivity was overwhelmed by the competing influences of temperature and salinity. The most compelling evidence that resistivity can be used to map hydrates is shown by Schwalenberg et al. (2005), who measure raised resistivities across several seismic blank zones (off Cascadia) thought to represent hydrate-bearing pipes.

In general, areas of hydrate formation are complex, and many other processes can complicate the interpretation of resistivity (carbonate formation, brine formation, pore-water freshening as hydrate dissociates, raised geotherms related to fluid advection); unless the hydrate is massive, its impact on the bulk resistivity will be modest to begin with, as is seen in ODP drilling (e.g., Hyndman et al., 1999).

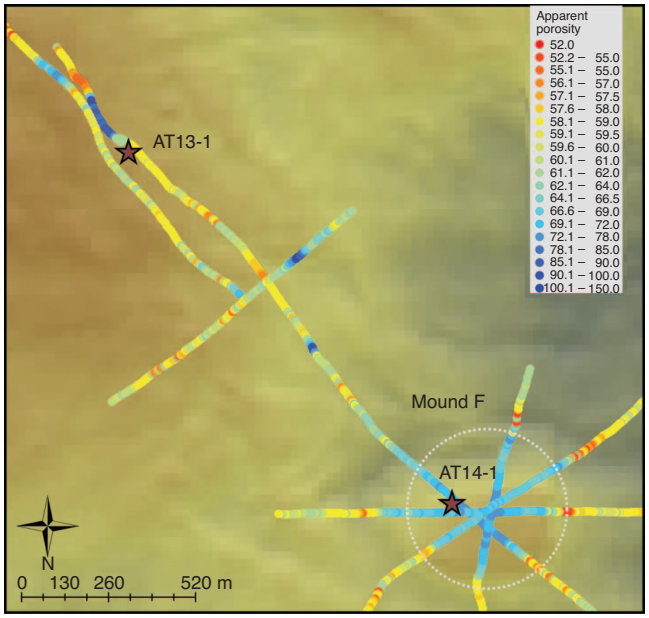

Figure 8. EM coverage across mound F in Atwater Valley, northern Gulf of Mexico (Ellis et al., 2005). The track lines of the EM system are shown color coded by the apparent porosities measured by the 13-m receiver (per values shown in the legend). Within the confines of mound F, the apparent porosities are raised. The locations of the two JIP drill holes are shown by the stars. Bathymetry data courtesy of WesternGeco.

FUTURE DIRECTIONS AND APPLICATIONS

In its current configuration, the towed magnetic-dipole array discussed in this paper offers the potential to address a number of outstanding issues, including mapping fluid seeps on the continental shelf and slope, addressing issues of slope stability, and mapping shallow gas hydrate occurrences. One area yet to be explored is the study of continental shelf submarine canyons. These features are important in their own right as a pathway for sediment dispersal from the shelf into the deep ocean. Little is known about their mechanisms of filling (e.g., Cronin et al., 2005), which has been shown to be dramatically different from those of terrestrial systems (Das et al., 2004); yet, this filling process has implications for the petroleum industry in areas where such features host oil and gas deposits (Mayall and Stewart, 2001). The near-seafloor structures of these features can be mapped using the EM system, with deeper properties inferred from these shallow analogs.

There are clearly targets for which the ability to look deeper into the seafloor is desirable. For example, deeper gas hydrate concentrations, trapped groundwater, channel sequences, and possibly sand injectites (e.g., Hurst et al., 2003). In principle, there is no reason why the system could not be extended to provide deeper penetration. The limit to this is probably a system of 400–500 m in length, comparable to the HED system operated by the University of Toronto (Yuan and Edwards, 2000; Schwalenberg et al., 2005). Beyond that, the most expedient approach is to transmit to seafloor instruments (e.g., Weitemeyer et al., 2006), at which point the system becomes less of a mapping tool, with data analysis requiring more complex 2D and 3D inversion schemes. Even with separations of 400–500 m, the likelihood is that more complex modeling of the data will be required than the simple 1D approach but which so far has proven satisfactory. Fortunately, with the boom in industry-related EM surveying, tools are being provided to allow this analysis, with more undoubtedly on the way.

CONCLUSIONS

We have discussed applications of a seafloor towed EM system that has been used over the last decade or so in a variety of continental shelf settings. Electrical resistivity measurement has proven to be a useful complement to other geophysical and sampling techniques. In some cases the EM system provides data where seismic surveys suffer from wipeout. The density of data provided in a typical survey is substantially greater than can be provided by coring and allows tighter estimates of sediment variability. The use of controlled-source EM techniques for deeper-probing industrial applications has not yet translated into interest in shallow studies, but the applications discussed in this paper may stimulate such interest.

ACKNOWLEDGMENTS

Clearly, the data presented in this paper would not have been possible without the early efforts of Nigel Edwards and Steve Cheesman, who built the first towed EM system, and without the work of Lawrie Law and Benoit St. Louis at the GSC, who turned it into a true surveying tool. Funding for the Eel River, New Jersey, and Martha's Vineyard surveys came from the Office of Naval Research, and we are particularly grateful for the support of Joe Kravitz. The National Science Foundation funded the construction of the WHOI EM system, which was carried out by John Bailey, Matthew Gould, and

Alan Gardner. Dan Lizarralde collected and processed chirp seismic data from Carolina. Ann Mulligan ran the hydrologic models for the North Carolina study. Funds for the Gulf of Mexico experiment came from the Deep Ocean Exploration Institute at WHOI, the Gas Hydrates Research Consortium run by the University of Mississippi, and the Department of Energy. Coworkers on the Gulf of Mexico project are Michelle Ellis, Debbie Hutchinson, and Pat Hart. Emrys Jones (Chevron/JIP) and Tim Collett are thanked for allowing us access to and permission to use JIP drilling data prior to publication. The manuscript benefitted from the comments of a large number of anonymous reviewers as well as assistance from the guest editors of this special section.

REFERENCES

Andrews, D., and A. Bennett, 1984, Measurements of diffusivity near the sediment-water interface with a fine scale resistivity probe: Geochimica et Cosmochemica Acta, **45**, 2169–2175.

Archie, G. E., 1942, The electrical resistivity log as an aid in determining some reservoir characteristics: Journal of Petroleum Technology, **5**, 1–8.

Baba, K., A. D. Chave, R. L. Evans, G. Hirth, and R. Mackie, 2006, Mantle dynamics beneath the East Pacific Rise at 17° S: Insights from the mantle electromagnetic and tomography (MELT) experiment: Journal of Geophysical Research, **111**, B02101; http://dx.doi.org/10.1029/2004JB003598.

Bailey, R. C., and S. Cheesman, 1992, L1 model norm inversion of resistive limit frequency-domain loop-loop electromagnetic data: 62nd Annual International Meeting, SEG, Expanded Abstracts, **62**, 420–422.

Baker, V. R., R. C. Kochel, J. E. Laity, and A. D. Howard, 1990, Spring sapping and valley network development, *in* C. G. Higgins and D. R. Coates, eds., Groundwater geomorphology: The role of subsurface water in earth-surface processes and landforms: Geological Society of America Special Publication 252, 235–365.

Beard, D. C., and P. K. Weyl, 1973, Influence of texture on porosity and permeability of unconsolidated sand: AAPG Bulletin, **57**, 349–369.

Bennett, R. H., W. R. Bryant, and G. Keller, 1981, Clay fabric of selected submarine sediments: Fundamental properties and models: Journal of Sedimentary Petrology, **51**, 217–231.

Bernabé, Y., W. F. Brace, and B. Evans, 1982, Permeability, porosity and pore geometry of hot-pressed calcite: Mechanics of Materials, **1**, 173–183.

Brooks, J. M., M. C. Kennicutt, R. R. Fay, T. J. MacDonald, and R. Sassen, 1984, Thermogenic gas hydrates in the Gulf of Mexico: Science, **223**, 696–698.

Cairns, G., R. L. Evans, and R. N. Edwards, 1996, A time domain electromagnetic survey of the TAG hydrothermal mound: Geophysical Research Letters, **23**, 3455–3458.

Cheesman, S. J., 1989, A short baseline transient electromagnetic method for use on the seafloor: Ph.D. thesis, University of Toronto.

Cheesman, S. J., R. N. Edwards, and A. D. Chave, 1987, On the theory of seafloor conductivity mapping using transient electromagnetic systems: Geophysics, **52**, 204–217.

Cheesman, S. J., L. K. Law, and B. St. Louis, 1993, A porosity survey in Hecate Strait using a seafloor electromagnetic profiling system: Marine Geology, **110**, 245–256.

Church, T. M., 1996, An underground route for the water cycle: Nature, **380**, 579–580.

Collett, T. S., A. Conte, L. L. Loh, H. F. Hoong, and D. S. Goldberg, 2005, Preliminary analysis of the downhole well logs from the Gulf of Mexico gas hydrate JIP cruise: EOS Transactions American Geophysical Union, **86**, OS31D–02.

Constable, S. C., R. L. Parker, and C. G. Constable, 1987, Occam's inversion: A practical algorithm for generating smooth models from electromagnetic sounding data: Geophysics, **52**, 289–300.

Cox, C. S., C. S. Constable, A. D. Chave, and S. C. Webb, 1986, Controlled source electromagnetic sounding of the oceanic lithosphere: Nature, **320**, 52–54.

Cronin, B. T., A. M. Akhmetzhanov, A. Mazzini, G. Akhmanov, M. Ivanov, and N. H. Kenyon, 2005, TTR-110 Shipboard scientists, morphology, evolution and fill: Implications for sand and mud distribution in filling deep-water canyons and slope channel complexes: Sedimentary Geology, **179**, 71–97.

Das, H. S., J. Imran, C. Pirmez, and D. Mohrig, 2004, Numerical modeling of flow and bed evolution in meandering submarine channels: Journal of Geophysical Research, **109**, C10009; http://dx.doi.org/10.1029/2002JC001518.

David, C., 1993, Geometry of flow paths for fluid transport in rocks: Journal of Geophysical Research, **98**, 12267–12278.

Davies, T. A., and J. A. Austin Jr., 1997, High-resolution 3D seismic reflection and coring techniques applied to late Quaternary deposits on the New Jersey shelf: Marine Geology, **143**, 137–149.

Davies, T. A, J. A. Austin Jr., M. B. Lagoe, and J. D. Milliman, 1992, Late Quaternary sedimentation of New Jersey: New results using 3D seismic profiles and cores: Marine Geology, **108**, 323–343.

Dickens, G. R., M. M. Castillo, and J. C. G. Walker, 1997, A blast of gas in the latest Paleocene: Simulating first-order effects of massive dissociation of oceanic methane hydrate: Geology, **25**, 259–262.

Edwards, R. N., 1997, On the resource evaluation of marine gas hydrate deposits using seafloor transient electric dipole-dipole methods: Geophysics, **62**, 63–74.

Ellis, M., R. L. Evans, D. R. Hutchinson, and P. Hart, 2005, An electromagnetic survey of the JIP drill sites in Atwater Valley: EOS Transactions American Geophysical Union, **86**, OS31D–07.

Evans, R. L., 1994, Constraints on the large scale porosity of young oceanic crust from seismic and resistivity data: Geophysical Journal International, **119**, 869–879.

———, 2001, Measuring the shallow porosity structure of sediments on the continental shelf: A comparison of an electromagnetic approach with cores and acoustic backscatter: Journal of Geophysical Research, **106**, 27047–27060.

Evans, R. L., S. C. Constable, M. C. Sinha, C. S. Cox, and M. J. Unsworth, 1991, Upper-crustal resistivity structure of the East Pacific Rise near 13°N: Geophysical Research Letters, **18**, 1917–1920.

Evans, R. L., L. K. Law, B. St. Louis, and S. Cheesman, 2000, Buried paleochannels on the New Jersey continental margin: Channel porosity structures from electromagnetic surveying: Marine Geology, **170**, 381–394.

Evans, R. L., L. K. Law, B. St. Louis, S. Cheesman, and K. Sananikone, 1999, The shallow porosity structure of the continental shelf of the Eel Shelf, northern California: Results of a towed electromagnetic survey: Marine Geology, **154**, 211–226.

Evans, R. L., and D. Lizarralde, 2003, Geophysical evidence for karst formation associated with offshore groundwater transport: An example from North Carolina: Geochemistry, Geophysics, Geosystems, **4**, 10.1029/2003GC000510.

Evans, R. L., M. C. Sinha, S. C. Constable, and M. J. Unsworth, 1994, On the electrical nature of the axial melt zone at 13°N on the East Pacific Rise: Journal of Geophysical Research, **99**, 577–588.

Gay, A., M. Lopez, P. Cochonat, M. Seranne, D. Levache, and G. Sermondadaz, 2006, Isolated seafloor pockmarks linked to BSRs, fluid chimneys, polygonal faults and stacked Oligocene-Miocene turbiditic palaeochannels in the Lower Congo Basin: Marine Geology, **226**, 25–40.

Goff, J. A., B. J. Kraft, L. A. Mayer, S. G. Shock, C. K. Sommerfield, H. C. Olson, S. P. S. Gulick, and S. Nordfjord, 2004, Seabed characterization on the New Jersey middle and outer shelf: Correlatability and spatial variability of seafloor sediment properties: Marine Geology, **209**, 147–172.

Goff, J. A., L. A. Mayer, P. Traykovski, I. V. Buynevich, R. Wilkens, R. Raymond, G. Glang, R. L. Evans, H. Olsen, and C. Jenkins, 2005, Detailed investigation of sorted bedforms, or "rippled scour depressions," within the Martha's Vineyard Coastal Observatory, Massachusetts: Continental Shelf Research, **25**, 461–484.

Goff, J. A., D. Orange, L. A. Mayer, and J. Hughes-Clarke, 1999, Detailed investigation of continental shelf morphology from a high resolution swath sonar survey over the Eel River basin, northern California: Marine Geology, **154**, 255–269.

Goff, J. A., R. A. Wheatcroft, H. Lee, D. E. Drake, D. J. P. Swift, and S. Fan, 2002, Spatial variability of shelf sediments in the STRATAFORM natural laboratory, northern California: Continental Shelf Research, **22**, 1199–1223.

Hamilton, E. L., and R. T. Bachman, 1982, Sound velocity and related properties of marine sediments: Journal of the Acoustical Society of America, **72**, 1891–1904.

Hashin, Z., and S. Shtrikman, 1962, A variational approach to the theory of effective magnetic permeability of multiphase materials: Journal of Applied Physics, **33**, 3125–3131.

Hoefel, F. G., and R. L. Evans, 2001, Impact of low salinity porewater on seafloor electromagnetic data: A means of detecting submarine groundwater discharge?: Estuarine, Coastal, and Shelf Science, **52**, 179–189.

Hovland, M., 2000, Are there commercial deposits of marine hydrates in ocean sediments?: Energy Exploration and Exploitation, **18**, 339–347.

Hovland, M., and O. T. Gudmestad, 2000, Potential influence of gas hydrate on seabed installations, *in* C. K. Paull and W. Dillon, eds., Natural gas hydrates: Occurrence, distribution and detection: American Geophysical Union Geophysical Monograph 124, 307–315.

Hurst, A., J. Cartwright, M. Huuse, R. Jonk, A. Schwab, D. Duranti, and B. Cronin, 2003, Significance of large-scale sand injectites as long-term fluid conduits: Evidence from seismic data: Geofluids, **3**, 263–274.

Hyndman, R. D., T. Yuan, and K. Moran, 1999, The concentration of deep sea gas hydrates from downhole electrical resistivity logs and laboratory data: Earth and Planetary Science Letters, **172**, 167–177.

Jackson, D. R., and K. B. Briggs, 1992, High-frequency bottom backscattering: Roughness versus volume scattering: Journal of the Acoustical Society of America, **92**, 962–977.
Jackson, P. D., K. B. Briggs, R. C. Flint, R. J. Holyer, and J. C. Sandidge, 2002, Two- and three-dimensional heterogeneity in carbonate sediments using resistivity imaging: Marine Geology, **182**, 55–76.
Jackson, P. D., D. Taylor-Smith, and P. N. Stanford, 1978, Resistivity-porosity-particle shape relationships for marine sands: Geophysics, **43**, 1250–1268.
Judd, A., 2004, Natural seabed gas seeps as sources of atmospheric methane: Environmental Geology, **46**, 988–996.
Kennicutt, M. C., J. M. Brooks, and G. J. Denoux, 1988, Leakage of deep, reservoired petroleum to the near surface on the Gulf of Mexico continental slope: Marine Chemistry, **24**, 39–59.
Kvenvolden, K. A., 1993, Gas hydrates — Geological perspective and global change: Reviews of Geophysics, **31**, 173–187.
Laity, J. E., and M. C. Malin, 1985, Sapping processes and the development of theater-headed valley networks on the Colorado Plateau: Geological Society of America Bulletin, **96**, 203–317.
MacGregor, L. M., S. C. Constable, and M. C. Sinha, 1998, The RAMESSES experiment III: Controlled source electromagnetic sounding of the Reykjanes Ridge at 57°45'N: Geophysical Journal International, **135**, 773–789.
MacGregor, L., M. Sinha, and S. Constable, 2001, Electrical resistivity structure of the Valu Fa Ridge, Lau Basin, from marine controlled source electromagnetic sounding: Geophysical Journal International, **146**, 217–236.
Madden, T. R., 1976, Random networks and mixing laws: Geophysics, **41**, 1104–1125.
Martin, W. R., M. Bender, M. Leinen, and J. Orchardo, 1991, Benthic organic carbon degradation and biogenic silica dissolution in the central equatorial Pacific: Deep-Sea Research, **38**, 1481–1516.
Mayall, M., and I. Stewart, 2001, The architecture of turbidite slope channels *in* S. I. Fraser, H. D. Johnson, A. J. Fraser, and A. M. Evans, eds., Petroleum geology of deepwater depositional systems — Advances in understanding 3D architecture: Geological Society of London.
Milkov, A. V., G. R. Dickens, G. E. Claypool, Y.-J. Lee, W. S. Borowski, M. E. Torres, W. Xu, H. Tomaru, A. M. Trehu, and P. Schultheiss, 2004, Co-existence of gas hydrate, free gas, and brine within the regional gas hydrate stability zone at the southern summit of Hydrate Ridge (Oregon margin): Evidence from prolonged degassing of a pressurized core: Earth and Planetary Science Letters, **222**, 829–843.
Milliman, J. D., Z. Jiezao, L. Anchun, and J. I. Ewing, 1990, Late Quaternary sedimentation on the outer and middle New Jersey continental shelf: Result of two local deglaciations: Journal of Geology, **98**, 966–976.
Moore, W. S., J. Krest, G. Taylor, E. Roggenstein, S. Joye, and R. Lee, 2002, Thermal evidence of water exchange through a coastal aquifer: Implications for nutrient fluxes: Geophysical Research Letters, **29**, 1704; http://dx.doi.org/10.1029/2002GL014923.
Moore, W. S., and T. J. Shaw, 1998, Chemical signals from submarine fluid advection onto the continental shelf: Journal of Geophysical Research, **103**, 21543–21552.
Mosher, D., and L. K. Law, 1996, Application of concurrent marine electromagnetic and marine seismic high resolution profiling, British Columbia, Canada: Journal of Environmental and Engineering Geophysics, **1**, 215–228.
Mulligan, A. E., R. L. Evans, and D. Lizarralde, 2007, The role of paleochannels in groundwater/seawater exchange: Journal of Hydrology, in press.
Nesbitt, B. E., 1993, Electrical resistivities of crustal fluids: Journal of Geophysical Research, **98**, 4301–4310.
Parker, R. L., 1994, Geophysical inverse theory: Princeton University Press.
Perkin, R. G., and E. L. Lewis, 1980, The practical salinity scale 1978: Fitting the data: IEEE Journal of Ocean Engineering, **OE-5**, 9–16.
Phillips, S. W., 1987, Hydrogeology, degradation of ground-water quality, and simulation of infiltration from the Delaware River into the Potomac aquifers, northern Delaware: U. S. Geological Survey Water-Resources Investigations Report 87-4185.
Quist, A. S., and W. L. Marshall, 1968, Electrical conductances of aqueous sodium chloride solutions from 0 to 800°C and at pressures to 4000 bars: Journal of Physical Chemistry, **71**, 684–703.
Roberts, J. N., and L. M. Schwartz, 1985, Grain consolidation and electrical conductivity in porous media: Physics Reviews B, **31**, 5990–5996.
Ruppel, C., G. R. Dickens, D. G. Castellini, W. Gilhooly, and D. Lizarralde, 2005, Heat and salt inhibition of gas hydrate formation in the northern Gulf of Mexico: Geophysical Research Letters, **32**; http://dx.doi.org/10.1029/2004GL021909.
Sassen, R., I. R. MacDonald, N. Guinasso, S. Joye, A. G. Requejo, S. T. Sweet, J. Alcala-Herrera, D. A. deFreitas, and D. R. Schink, 1998, Bacterial methane oxidation in seafloor gas hydrate: Significance to life in extreme environments: Geology, **26**, 851–854.
Schwalenberg, K., E. C. Willoughby, R. Mir, and R. N. Edwards, 2005, Marine gas hydrate electromagnetic signatures in Cascadia and their correlation with seismic blank zones: First Break, **23**, 57–63.
Schwartz, L. M., and S. Kimminau, 1987, Analysis of electrical conduction in the grain consolidation model: Geophysics, **52**, 1402–1411.
Shankland, T. J., and H. S. Waff, 1974, Conductivity in fluid bearing rocks: Journal of Geophysical Research, **79**, 4863–4868.
Sheremet, A., and G. W. Stone, 2003, Observations of nearshore wave dissipation over muddy sea beds: Journal of Geophysical Research, **108**, 3357; http://dx.doi.org/10.1029/2003JC001885.
Swarzenski, P. W., C. D. Reich, R. M. Spechler, J. L. Kindinger, and W. S. Moore, 2001, Using multiple geochemical tracers to characterize the hydrogeology of the submarine spring off Crescent Beach, Florida: Chemical Geology, **179**, 187–202.
Uchupi, E., and R. N. Oldale, 1994, Spring sapping origin of the enigmatic relict valleys of Cape Cod, Martha's Vineyard and Nantucket Islands, Massachusetts: Geomorphology, **9**, 83–95.
Weitemeyer, K. A., S. Constable, K. Key, and J. Behrens, 2006, First results from a marine controlled-source electromagnetic survey to detect gas hydrates offshore Oregon: Geophysical Research Letters, **33**; http://dx.doi.org/10.1029/2005GL024896.
Wheatcroft, R. A., J. C. Borgeld, R. S. Born, D. E. Drake, E. L. Leithold, C. A. Nittrouer, and C. K. Sommerfield, 1996, The anatomy of an oceanic flood deposit: Oceanography, **9**, 158–162.
Wilson, A. M., and C. Ruppel, 2005, Impact of shallow convection on the gas hydrate reservoir in the Gulf of Mexico salt tectonics province: EOS Transactions American Geophysical Union, **86**, OS41–06.
Wong, P. Z., J. Koeplik, and J. P. Tomanic, 1984, Conductivity and permeability of rocks: Physics Reviews B, **30**, 6606–6614.
Xu, W., and C. Ruppel, 1999, Predicting the occurrence, distribution, and evolution of methane gas hydrate in porous marine sediments: Journal of Geophysical Research, **104**, 5081–5095.
Yuan, J., and R. N. Edwards, 2000, The assessment of marine gas hydrate through electrical remote sounding: Hydrate without a BSR?: Geophysical Research Letters, **27**, no. 16, 2397–2400.
Zhang, S., M. S. Paterson, and S. F. Cox, 1994, Porosity and permeability evolution during hot isostatic pressing of calcite aggregates: Journal of Geophysical Research, **99**, 15741–15760.
Zhu, W., C. David, and T.-F. Wong, 1995, Network modeling of permeability evolution during cementation and hot isostatic pressing: Journal of Geophysical Research, **100**, 15451–15464.